

1-30-2013

# Aerosol synthesis and Rietveld refinement of Pd<sub>2</sub>Zn

Jim Fitch

Follow this and additional works at: [https://digitalrepository.unm.edu/nsms\\_etds](https://digitalrepository.unm.edu/nsms_etds)

---

## Recommended Citation

Fitch, Jim. "Aerosol synthesis and Rietveld refinement of Pd<sub>2</sub>Zn." (2013). [https://digitalrepository.unm.edu/nsms\\_etds/29](https://digitalrepository.unm.edu/nsms_etds/29)

This Thesis is brought to you for free and open access by the Engineering ETDs at UNM Digital Repository. It has been accepted for inclusion in Nanoscience and Microsystems ETDs by an authorized administrator of UNM Digital Repository. For more information, please contact [disc@unm.edu](mailto:disc@unm.edu).

James A Fitch

*Candidate*

---

Nanoscience and Microsystems

*Department*

---

This thesis is approved, and it is acceptable in quality and form for publication:

*Approved by the Thesis Committee:*

Abhaya K Datye , Chairperson

---

Boris Kiefer

---

Ying-Bing Jiang

---

# **Aerosol Synthesis and Rietveld Refinement of Pd<sub>2</sub>Zn**

by

**James Allen Fitch**

**B.S. Mechanical Engineering University  
of New Mexico, 2010**

THESIS

Submitted in Partial Fulfillment of the  
Requirements for the Degree of

**Masters of Science  
Nanoscience and Microsystems**

The University of New Mexico  
Albuquerque, New Mexico

**December, 2012**

# **Aerosol Synthesis and Rietveld Refinement of Pd<sub>2</sub>Zn**

by

**James Allen Fitch**

**B.S. Mechanical Engineering, University  
of New Mexico, 2010**

**M.S. Nanoscience and Microsystems, University  
of New Mexico, 2012**

## **Abstract**

PdZn catalysts have been proven to be a viable option to replace current Cu catalysts for methanol steam reforming. The change in selectivity to CO<sub>2</sub> that makes this a possibility has been attributed to the formation of tetragonal  $\beta_1$ -PdZn at treatment temperatures of 500°C. Through the course of studying the phase evolution of the 1:1 PdZn, it was seen that an intermediate Pd<sub>2</sub>Zn phase formed at intermediate temperatures in the course of the reduction from room temperature to 600°C. This phase had not been previously reported by any group currently studying the PdZn system. The discovery of this phase prompted this study in order to isolate and confirm the structure of 2:1 Pd<sub>2</sub>Zn.

## Table of Contents

<b>Abstract.....</b>	<b>iii</b>
<b>Table of Contents .....</b>	<b>iv</b>
<b>List of Figures.....</b>	<b>vi</b>
<b>List of Tables .....</b>	<b>viii</b>
<b>Nomenclature .....</b>	<b>ix</b>
<b>Introduction.....</b>	<b>1</b>
1.1 Methanol Fuels for Portable Power.....	1
1.2 Supported Copper Catalysts .....	2
1.3 PdZn Catalysts.....	4
1.4 Objectives.....	6
<b>Literature Review .....</b>	<b>7</b>
2.1 Supported PdZn Catalysts .....	7
2.2 Unsupported PdZn catalysts.....	9
2.3 Reported Pd <sub>2</sub> Zn structure .....	11
<b>3. Experimental Methods .....</b>	<b>12</b>
3.1 Synthesis.....	12
3.2 Characterization .....	13
<b>Results and Discussion.....</b>	<b>16</b>
4.1 As-Prepared Oxide .....	16
4.2 Sample Reduced in H <sub>2</sub> at 500°C.....	21
4.3 Sample Reduced in H <sub>2</sub> at 450°C .....	23
<b>Conclusions.....</b>	<b>32</b>

**Future Work..... 33**

**References..... 34**

## List of Figures

Figure 1. The comparison of loss of reactivity over time between a conventional Cu catalyst and a Pd/ZnO supported catalyst. Plot from Stability of bimetallic PdZn catalysts for steam reforming of methanol, Travis Conant, Journal of Catalysis, 2008.....	3
Figure 2. Synchrotron XRD data of a 1:1 PdZn catalyst showing the existence of Pd <sub>2</sub> Zn. DFT also confirms the formation of Pd <sub>2</sub> Zn at these temperatures .....	5
Figure 3. Figure 3. XRD patterns for Zn modified catalysts. (a)Pd/Zn/SiO <sub>2</sub> ; (b)Pd/Zn/Al <sub>2</sub> O <sub>3</sub> ; (c)Pd/Zn/MgO; (d) pd/Zn/ZrO <sub>2</sub> ; (e) Pd/Zn/MgO; (f) Pd/Zn/AC. Plot form Iwasa et al, Applied Catalysis A, 248 (2003) 153-160.....	8
Figure 4. Selectivity and reactivity of Pd on various supports with and without the presence of Zn. Iwasa et al. Applied Catalysis A 248 (2003) 153-160. ....	9
Figure 5. Schematic of the Aerosol Synthesis method. ....	9
Figure 6. SEM image of as-prepared Pd <sub>2</sub> Zn.....	16
Figure 7. X-ray powder diffraction and Rietveld Refinement results for as-prepared Pd <sub>2</sub> Zn.....	17
Figure 8. TGA analysis of sample A and reference PdO and ZnO in air. ....	18
Figure 9. XRD of the reference Zn sample shows the absence of ZnO peaks indicating that the aerosol method actually produced Zn nitrate. ....	19
Figure 10. TGA analysis of Sample A and Reference PdO and ZnO in H <sub>2</sub> .....	21
Figure 11. Figure 11. X-ray powder diffraction and Rietveld Refinement of sample A after eight hour reduction at 500C in flowing H <sub>2</sub> . ....	21
Figure 12. Sample B reduced for four hours at 450C in flowing H <sub>2</sub> . ....	24

Figure 13. X-ray powder diffraction and Rietveld Refinement of sample B after reduction at 450C for eight hours in flowing H <sub>2</sub> .....	25
Figure 14. Comparison between the XRD patterns of sample A and sample B.....	26
Figure 15. Electron microprobe analysis of Sample B after an eight hour reduction at 450C in flowing H <sub>2</sub> .....	27
Figure 16. Low magnification TEM of sample B after being sectioned on an ultramicrotome. ...	28
Figure 17. Comparison of the diffraction patterns of $\alpha$ -(Pd,Zn) and Pd <sub>2</sub> Zn.....	29
Figure 18. Indexing of the diffraction pattern of $\alpha$ -(Pd,Zn) .....	30
Figure 19. Indexing of the diffraction pattern cast by Pd <sub>2</sub> Zn. ....	31

## List of Tables

Table 1. Structure and phase composition of sample A as determined by Rietveld Refinement.....	22
Table 2. Structure and phase composition of Sample B as determined by Rietveld Refinement.....	25

## Nomenclature

BET	Brunauer-Emmett-Teller Surface Area Analysis
EDS	Energy Dispersive Spectroscopy
fcc	Face Centered Cubic
GSAS	General Structural Analysis Systems
HRTEM	High Resolution Transmission Electron Microscopy
ICDD	International Center for Diffraction Data
ICP	Inductively Coupled Plasma Spectroscopy
ID	Inner Diameter
MSR	Methanol Steam Reforming
OD	Outer Diameter
PEMFC	Proton Exchange Membrane Fuel Cell
SEM	Scanning Electron Microscope
TEM	Transmission Electron Microscope
TGA	Thermogravimetric Analysis
Wh/L	Watt Hours per Liter
XRD	X-ray Diffraction

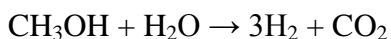
## Introduction

### 1.1 Methanol Fuels for Portable Power

The current electronics market has driven developers to design continually smaller and lighter devices. As anyone that has ever carried a laptop computer for any period of time knows, a large portion of the weight of the device is in the battery. This has created an increased interest in not only lighter components, but lighter and more efficient power sources as well. One potential power supply that could meet these needs is a Proton Exchange Membrane Fuel Cell (PEMFC). This technology was studied at length by Yoshihiro Kawamura at Kogakuin University. (Kawamura, 2006) It has been stated that these fuel cells are capable of twelve times the gravimetric energy density of conventional lithium ion batteries. (Dyer, 2002) This means that a fuel cell of this type would provide a greater deal of power while contributing much less weight to the overall device. Since these fuel cells are powered by Hydrogen, we are now faced with the problem of finding suitable fuels to generate Hydrogen.

Alcohols have been shown to have a very high energy density, and power systems based on fuel cells are reported to have volumetric energy densities of up to 2500 Wh/L for liquid Hydrogen or 5000 Wh/L for Methanol, compared to 400 Wh/L lithium ion batteries. (Dyer, 2004) Methanol is a suitable fuel, but to use methanol for a fuel cell the hydrogen must first be extracted. The chemical reaction that makes this possible is the Steam Reforming of Methanol. Methanol Steam Reforming (MSR) is the process by which Methanol and water are reacted to produce hydrogen and carbon dioxide. Because methanol has a single carbon atom, we do not have to break any carbon-carbon bonds.

Furthermore, the carbon is already bound to one oxygen in methanol. Therefore, the reaction of methanol with water can take place at relatively low temperatures compared to other alcohols or other hydrocarbons. Ethanol also has a carbon-oxygen bond, but ethanol steam reforming requires that the carbon-carbon bond be broken. The equation below shows the stoichiometry for this reaction.



Reformers tested for integrated portable power fuel cell devices operate in the range of 230°C to 320°C. (Farrauto, 2011) Although, this temperature still appears high for a portable device MEMS technology had provided a method of miniaturizing the reactor in a way as to meet realistic operating conditions. (Kawamura, 2006) Aside from the low reaction temperature, Methanol has another desirable characteristic as a hydrogen carrier. The lack of sulfur means that it is a clean as well as efficient energy source.

## 1.2 Supported Copper Catalysts

The industry standard catalysts for MSR have been Cu catalysts, typically Cu-Zn-Alumina used in methanol synthesis and water gas shift reactions. (Farrauto, 2011) These catalysts have several drawbacks, most notably, their tendency to lose activity. The method of failure for these catalysts is predominantly that they suffer from copper sintering at temperatures above 260°C. Cu catalysts are also highly pyrophoric, which means they oxidize upon contact with air. Oxidation of these catalysts severely affects their reactivity. Once Cu catalysts have lost their activity from either sintering or oxidation, they are nearly impossible to regenerate.

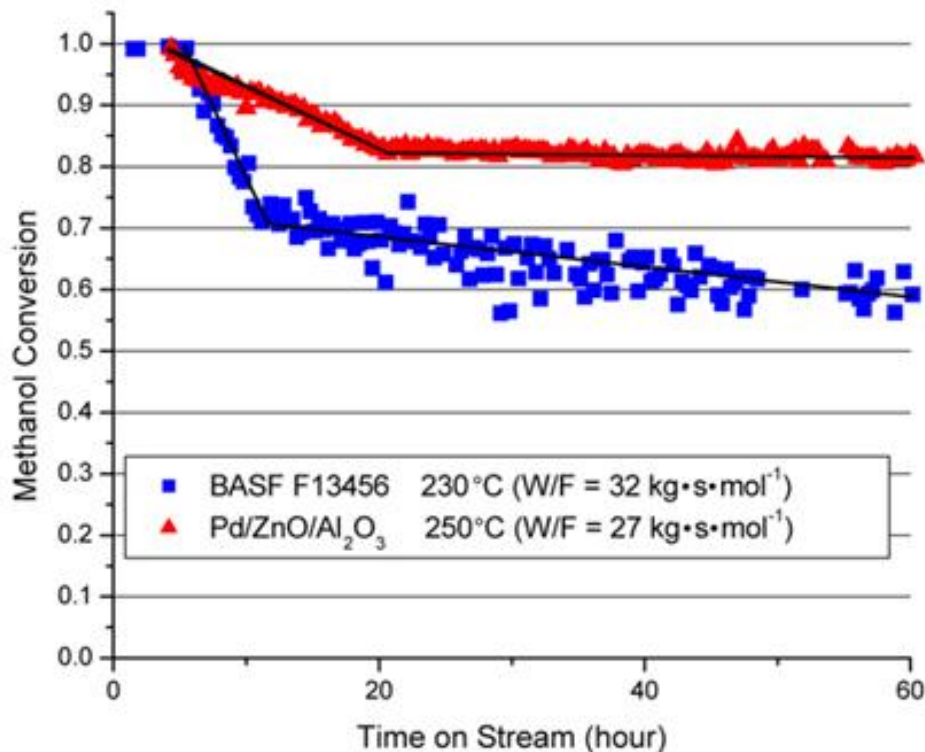


Figure 1. The comparison of loss of reactivity over time between a conventional Cu catalyst and a Pd/ZnO supported catalyst. Plot from Stability of bimetallic PdZn catalysts for steam reforming of methanol, Travis Conant, Journal of Catalysis, 2008.

As the prototype technologies incorporating hydrogen as a fuel source become closer to reality, it has become necessary to find more stable catalysts that facilitate the chemical reactions necessary to produce the required volume of hydrogen over a reasonable device lifetime. One of the primary replacement candidates is a Pd based catalyst. Figure 1 shows a comparison of reactivity over time between a conventional copper catalyst currently in use in industry for MSR, and a supported PdZn catalyst. The loss of reactivity of the copper catalyst is dramatic when it is compared to the PdZn system. This would severely limit the usefulness of MSR as a means of powering personal electronic devices, as the duty cycle expected of these machines is substantial.

These PdZn catalysts were proven to be able to remedy the rapid deactivation exhibited by Cu supported catalysts. The pyrophoric nature of Cu catalysts, as well as their ease of sintering not only affected the overall useful lifetime of the catalyst, but meant that once these catalysts were deactivated they were permanently destroyed. Supported PdZn catalysts have shown that, although, the active alloy can be broken up into PdO and ZnO, the alloy phase can be reduced and restored to a functioning state in-situ.

### 1.3 PdZn Catalysts

PdZn catalysts have come under a great deal of attention over the past several years as a possibility of replacing currently available supported Cu catalysts for Methanol Steam Reforming. Primarily, the interest has been in the 1:1 tetragonal  $\beta$ -phase PdZn, which has been shown to be the catalytically active phase for MSR. (Halevi, 2010) Throughout the course of the work being conducted on this system both in the United States and abroad it has been determined that reduction temperatures as high as 500°C are needed to achieve the proper selectivity. (Iwasa, 2003) Heating to high temperatures causes grain growth and coarsening, which decreases the surface area. Catalysis is a surface phenomenon, so it is important to keep the highest surface area to have the most active catalyst.

Although, the aerosol route has been employed to prepare phase pure unsupported powder catalysts, the steps that lead to the synthesis of the final product have not been investigated. Understanding these steps would allow us to develop the optimal treatment temperature to produce high surface area, durable powder catalysts. Therefore, the objective of this study was to understand the phase transformations to convert the initial

oxide powder into the final intermetallic phase pure material. In order to begin the study of the phase transformation of the PdZn system a 1:1 oxide was prepared using the method outlined in Eric Peterson's publication on the structural refinement of PdZn. (Peterson, 2010) This oxide was reduced in order to confirm that it yields the  $\beta$ -phase after treatment. The sample was taken to Brookhaven National Labs for performing in-situ study of phase transformation. A sample of the 1:1 oxide was enclosed in a quartz capillary, and progressively heated from room temperature to 600°C in flowing  $H_2$ .

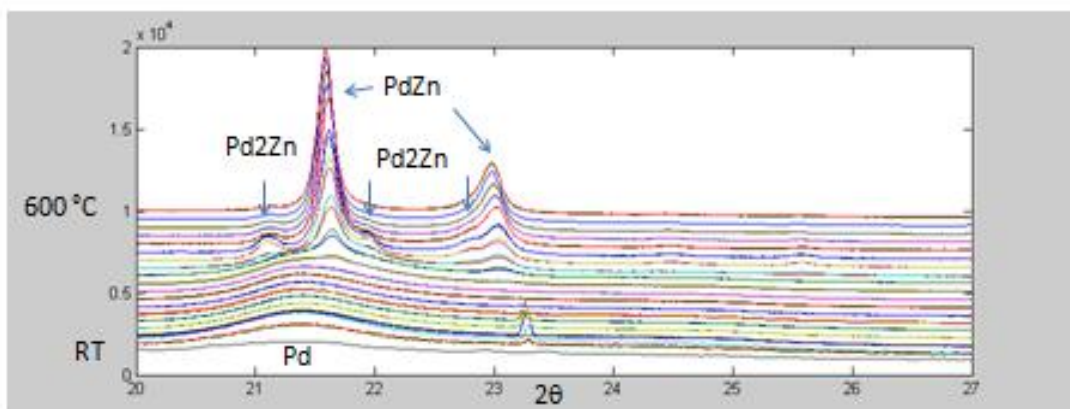


Figure 2. Synchrotron XRD data of a 1:1 PdZn catalyst showing the existence of  $Pd_2Zn$ . DFT also confirms the formation of  $Pd_2Zn$  at these temperatures

Figure 2 shows the XRD data from this study. At temperatures of 325°C to 450°C we detected a phase not seen previously in published work. These peaks could be indexed to a  $Pd_2Zn$  phase. It appears that this  $Pd_2Zn$  phase formed before the material transformed into the tetragonal PdZn phase. To date, no group currently working on the PdZn system has reported this  $Pd_2Zn$  phase, possibly because its formation occurs at lower temperatures than commonly used for the synthesis of 1:1 PdZn catalysts. Since the properties and the structure of the  $Pd_2Zn$  phase are not known it was decided to focus on the synthesis and characterization of this phase.

## 1.4 Objectives

The specific objectives of this study are as follows:

1. Determine the optimal conditions to produce a phase pure Pd<sub>2</sub>Zn sample.
2. Perform a Rietveld Refinement to determine the structure of this phase.
3. Develop a method for studying aerosol derived particles in the TEM.
4. Perform TEM analysis to confirm the Rietveld Results.

## Literature Review

### 2.1 Supported PdZn Catalysts

Investigation into Pd catalysts began in an attempt to find a suitable replacement for supported Cu catalysts for steam reforming of methanol. (Iwasa, 2003) Although, Pd and other group 8-10 metals such as Pd, Pt, and Ni facilitate the decomposition of Methanol, they form CO rather than CO<sub>2</sub>. Although these metals exhibit good thermal stability for conversion of methanol, their selectivity for CO makes them unsuitable, since CO is a poison for Platinum catalysts used in fuel cells. (Iwasa, 2003) Iwasa's study was conducted using Pd catalysts on various supports. This work shows that the support used had a significant contribution in determining the selectivity of a catalyst, however, the largest contributing factor affecting the selectivity towards CO was the addition of Zn. It was hypothesized that this change in behavior could be attributed to PdZn alloys forming on the surface of the Pd catalysts under both reduction and reaction conditions. Further work done on Pd/Zn/Al<sub>2</sub>O<sub>3</sub> supported catalysts, shows that the phases Pd and PdZn in addition to the supports were present after reduction, and during reaction conditions. (Conant, 2008) The background contribution of the support makes structural analysis of these phases difficult. Figure 3 illustrates this problem, since a large portion of structural analysis done through XRD is based on relative peak intensities. The low intensity, broad peaks of the phase in question superimposed over the peaks of the support make it difficult to quantify the relative amounts of the different phases. Overlapping peaks makes it difficult to deconvolute the active phase from the support.

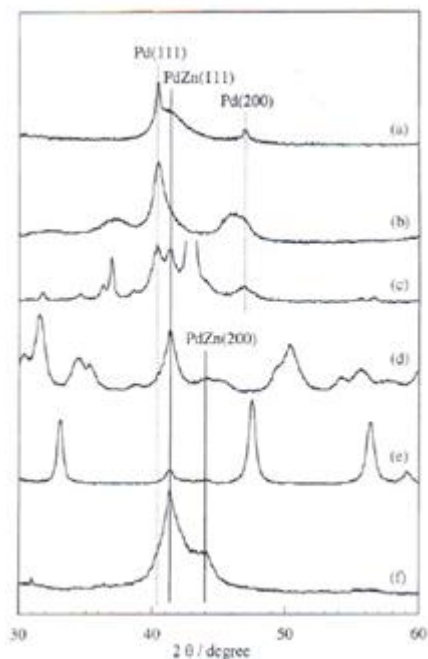
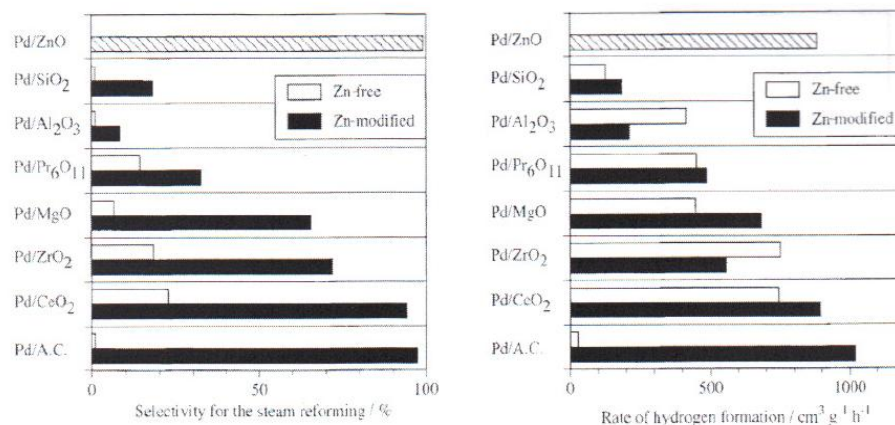


Figure 3. Figure 3. XRD patterns for Zn modified catalysts. (a)Pd/Zn/SiO<sub>2</sub>; (b)Pd/Zn/Al<sub>2</sub>O<sub>3</sub>; (c)Pd/Zn/MgO; (d) Pd/Zn/ZrO<sub>2</sub>; (e) Pd/Zn/MgO; (f) Pd/Zn/AC. Plot from Iwasa et al, Applied Catalysis A, 248 (2003) 153-160.

The common element that came out of the studies performed on supported PdZn catalysts is that the formation of alloy phase PdZn was believed to be the driving force behind the change in selectivity from CO to CO<sub>2</sub>. As stated above, testing this hypothesis using supported catalysts is difficult due to peak overlap. Hence, the interest in producing unsupported catalysts of the same phase and composition as the alloys produced on the surface of the ZnO support during reaction. Figure 4 shows the increase in selectivity and reactivity of Pd on various supports as the Zn is added.



from: Iwasa et al. *Appl. Catalysis A* **248** (2003) 153-160.

**Figure 4.** Selectivity and reactivity of Pd on various supports with and without the presence of Zn. Iwasa et al. *Applied Catalysis A* **248** (2003) 153-160.

## 2.2 Unsupported PdZn catalysts

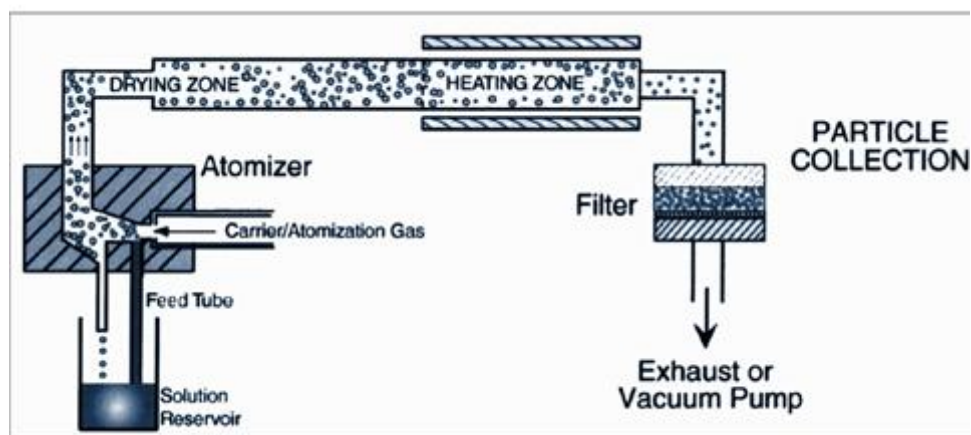


**Figure 5.** Schematic of the Aerosol Synthesis method.

UNM had developed a method of producing unsupported metallic catalysts of a desired composition through an aerosol route. Figure 5 shows a schematic of this process. This method involves passing an aerosolized metal precursor solution through a furnace at temperatures high enough to dry the aerosol droplets, and decompose the nitrates from the precursor. This method will be discussed in the chapter on experimental

methods. Previous to using the aerosol method, the nitrate precursor solution was dried to form the oxide, and then collected. Using this drying method left behind as much as 10% ZnO. (Halevi, 2010) On the other hand, using the aerosol method at compositions on or near the 50 atom% Zn led to the formation of phase pure of  $\beta_1$ -phase PdZn. There are many possible phases in the PdZn system, but this study is devoted to the formation of phase containing 33 at% Zn (Figure 5), hence we will next discuss the Pd rich half of the PdZn phase diagram.

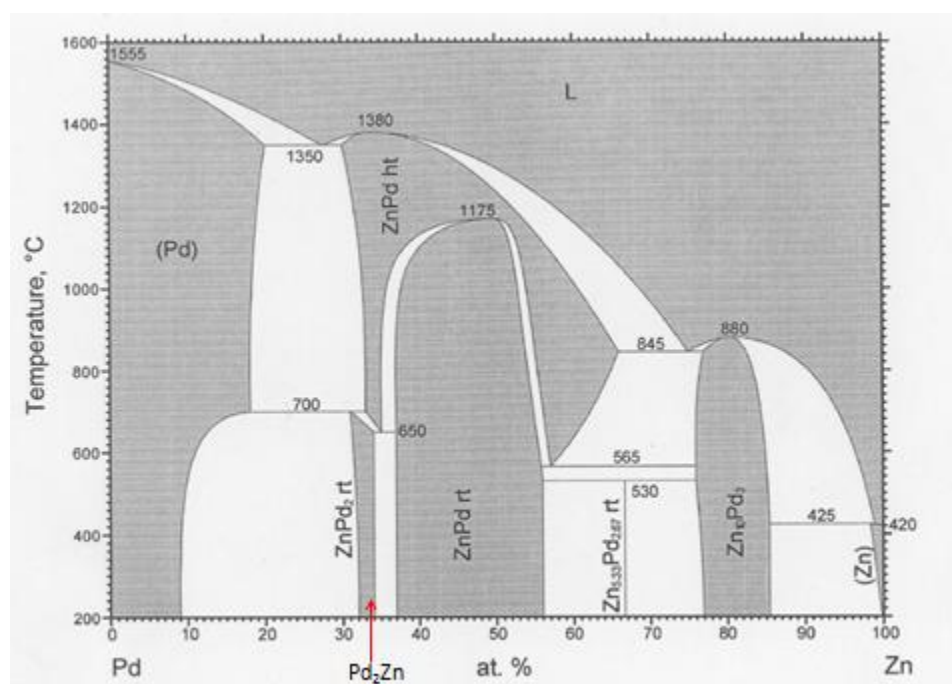


Figure 5. Phase diagram for the PdZn system. Phase diagram reported by Massalski et al.

PdZn shows three stable regions in the Pd rich portion of the diagram. This holds true from room temperature up to 500°C, which is the highest reduction temperature used in this study. The phase present from 0 to approximately 10 at% Zn is referred to as  $\alpha$ -Pd. This is solid solution of Pd and Zn with the Zn incorporated into the fcc Pd structure. The reactivity of this phase was published 2012, and it had shown unfavorable selectivity

for MSR. (Halevi, 2012) The region of the diagram from nominally 37 to 56 atom% Zn is tetragonal  $\beta_1$ -PdZn. To date this structure has been the only phase in the PdZn system that has shown proper selectivity for MSR. (Halevi, 2010) Aside from the immiscible regions, Pd<sub>2</sub>Zn is the only portion of the phase diagram that has not been investigated. Since the Pd<sub>2</sub>Zn lies between the  $\alpha$ -(Pd,Zn) which is selective to CO, and  $\beta_1$ -PdZn which is selective to CO<sub>2</sub>, it is of interest to determine the performance of this phase, which has yet been studied. If the Pd<sub>2</sub>Zn shows improved selectivity it may provide a means of creating an MSR catalyst with a higher surface area than possible with the  $\beta$ -phase powders, since the formation temperature appears to be lower.

### 2.3 Reported Pd<sub>2</sub>Zn structure

Although, this phase has not been seen through the course of the study of PdZn, it has been documented previously. A research group from North Carolina had published a structure in a 1963 article. (Stadelmaier, 1963) This structure has been used to describe the 2:1 region assigned to the existing PdZn phase diagram. The Pd<sub>2</sub>Zn is similar to the structure of Co<sub>2</sub>Si. More recently Armbruster et al. have also described the Pd<sub>2</sub>Ga phase which has the same structure as the Co<sub>2</sub>Si. This phase of Pd and Ga has been shown to have the Pnma space group, and unit cell  $a=5 \text{ \AA}$ ,  $b=4 \text{ \AA}$ , and  $c=7 \text{ \AA}$ . It is worth mentioning that it was found that the 2:1 ratio of Pd and Ga was the most selective catalyst for Acetylene Hydrogenation. (Armbruster, 2010).

### 3. Experimental Methods

#### 3.1 Synthesis

Catalysts were prepared using Aldrich Pd(NO<sub>3</sub>)<sub>2</sub> (Aldrich stock number 380040) solutions and Zn(NO<sub>3</sub>)<sub>2</sub>·6H<sub>2</sub>O salt (Aldrich Stock Number 228737). The 4.5 wt% Pd solution was used as received, while the Zn salt was dissolved in 10 wt% Nitric Acid. The precursor solution was mixed to yield a concentration of 33 at% Zn.

Precursor solutions were prepared in a standard 250mL Nalgene bottle, and partially submerged in a water bath in a Walgreens ultrasonic humidifier (model #500379). The ultra-sonic waves generated by the humidifier propagate through the Nalgene bottle producing a mist composed of droplets of the metal feed solution

This aerosol is then drawn through a 2.54cm OD quartz tube using lab air as a carrier gas. The quartz tube is mounted within a 80cm long three zone tube furnace. All three zones of the furnace were set to produce a temperature of 700°C. The lab air was used as a carrier gas to carry the aerosol through the furnace. A vacuum pump at the outlet served to create a total flow rate of 1 L/m. The flow rate and temperature of the furnace was set to ensure the complete decomposition of the nitrates to form a mixed oxide of Pd and Zn. Upon exiting the furnace, the powders were collected using 0.1 μm Pall Neoprene Supor-200 membrane filter, housed in a Gelman Sciences 120mm stainless steel filter housing.

A typical run was conducted using 75mL of precursor solution, and left to run overnight. After the solution in the Nalgene bottle had been exhausted, the filter was removed from the housing and the sample was collected for analysis. The sample was

collected by scraping the powder from the filter with a spatula, and storing it in a glass sample vial. This is the as-prepared oxide form of the PdZn catalyst. The collected powders were then packed into a 0.25in OD quartz tube, and treated in flowing H<sub>2</sub>. The gas used was 7% H<sub>2</sub> in N<sub>2</sub>, which was purified by passing through an oxy-trap to get rid of any traces of O<sub>2</sub>. After the quartz tube was connected to inlet gas, it was flushed with the flowing H<sub>2</sub> for five minutes to get rid of the residual air in the tube. All heat treatments were done by ramping the furnace to the desired temperature at a rate of ten degrees per minute, and then holding at that temperature for the entire reduction time. After the treatment time was reached the furnace was allowed to cool naturally, while still flowing H<sub>2</sub>. After reaching room temperature the flow of H<sub>2</sub> was stopped, and the tube was flushed with N<sub>2</sub>, and the opened to remove the sample. The air exposed sample was saved in vials for further analysis.

### 3.2 Characterization

The as-prepared powders were initially examined in a Hitachi S-5200 SEM at an accelerating voltage of 20kV. Samples of the powder were dispersed on double stick carbon tape mounted on an aluminum sample holder. SEM was used to determine the morphology and particle sizes of the as-prepared sample. EDS also provides qualitative elemental analysis.

Quantitative elemental analysis was performed by several methods to ensure that the samples were of the right stoichiometry before further heat treatments were performed. Inductively-coupled plasma spectroscopy was performed on the as-prepared material of Sample A. This was done using a PerkinElmer Optima 5300DV Inductively Coupled Plasma (ICP) Spectrometer. In order to get the proper data from the sample

0.5g of it was dissolved in aqua regia, and heated to 95°C until fully dissolved. The sample was diluted 1000 times, and analyzed by atomic absorption spectroscopy.

Thermogravimetric analysis was also used to determine the changes caused by heat treatment in air and H<sub>2</sub>/N<sub>2</sub>. This analysis was conducted using a TA model STQ600 Thermal Analyzer. Reference samples of both ZnO and PdO were prepared through the aerosol route. The samples were also analyzed using a JEOL 8200 microprobe operating at 20 kV and 20 nA. For this analysis it was necessary to embed the powder in epoxy, and to create a polished surface which was carbon coated before analysis.

X-ray diffraction was performed to determine the nature of the phases in both the as-prepared state as well as after H<sub>2</sub> reduction. The XRD patterns were acquired using a Scintag PAD V diffractometer operated at an accelerating voltage of 40 kV. Cu K $\alpha$  x-rays were used for all structural studies in this experiment, and the wavelength used for all relevant refinements and calculations was 1.5040562 Å. A graphite monochromator was used to remove Cu K- $\beta$  radiation. The samples were placed in a zero background holder. The sample holder was a quartz crystal polished and mounted in an orientation which does not produce any diffraction pattern from the quartz. It takes approximately 50 mg to fill the machined groove in the holder. These powders are fine, so they do not need to be ground. The sample was smoothed to be even with the surface of the holder using a standard microscope slide. The patterns were collected through 2°-95° 2 $\theta$  degrees with sampling points every 0.02 degrees, and a time of 12 seconds per point. XRD patterns were analyzed by Rietveld Refinement using the software program General Structural Analysis Systems (GSAS). GSAS is a collection of programs compiled to analyze x-ray and neutron diffraction data of both powders and single crystals.

To perform TEM analysis the powder samples were also embedded in epoxy and cross-sectioned in an ultramicrotome. This was done using a RMC products MTXL ultramicrotome. The diamond knife used to cut the samples was Diatome size 2.1 diamond knife, with a knife angle of  $45^{\circ}$ . The samples were dispersed in Electron Microscopy Sciences #1232 embedding resin, and cast in Beem size #00 embedding capsules. These epoxy molds were cured at  $80^{\circ}\text{C}$  for eight hours to harden the epoxy. After hardening, the molds were taken to the ultramicrotome, and shaped with a glass knife if needed prior to being sectioned with the diamond knife. The sample section thickness was set to 50 nm, and the sections were allowed to float on water before being gathered on SPI #02450-AB Cu holey carbon TEM grids. The cross-sectioned samples were also viewed in the Hitachi-5200 SEM to determine the quality of the thin sections. For the SEM analysis, the TEM grids were placed in a custom made sample holder that consisted of an aluminum body machined with a recess of the same diameter as the outer diameter as the standard SPI Cu grid, and a bore at the center of this recess to allow the beam to pass through.

As a final step in the characterization process, the samples were examined in a TEM. These analyses were performed on a JEOL 2010F TEM at beam energy of 200 keV. The samples were viewed using low magnification TEM and images were recorded with a GATAN Coolsnap Camera. The EDS system used was an Oxford Instruments ISIS/INCA energy dispersive x-ray spectroscopy (EDS) system with an Oxford Pentafet Ultrathin Window (UTW) Detector.

## Results and Discussion

In this work two PdZn samples of nominally the same compositions were prepared using identical methods, and treated at different temperatures. The precursor solutions were prepared, using the method described in the previous chapter, using a 2:1 atomic ratio of Pd and Zn.

### 4.1 As-Prepared Oxide

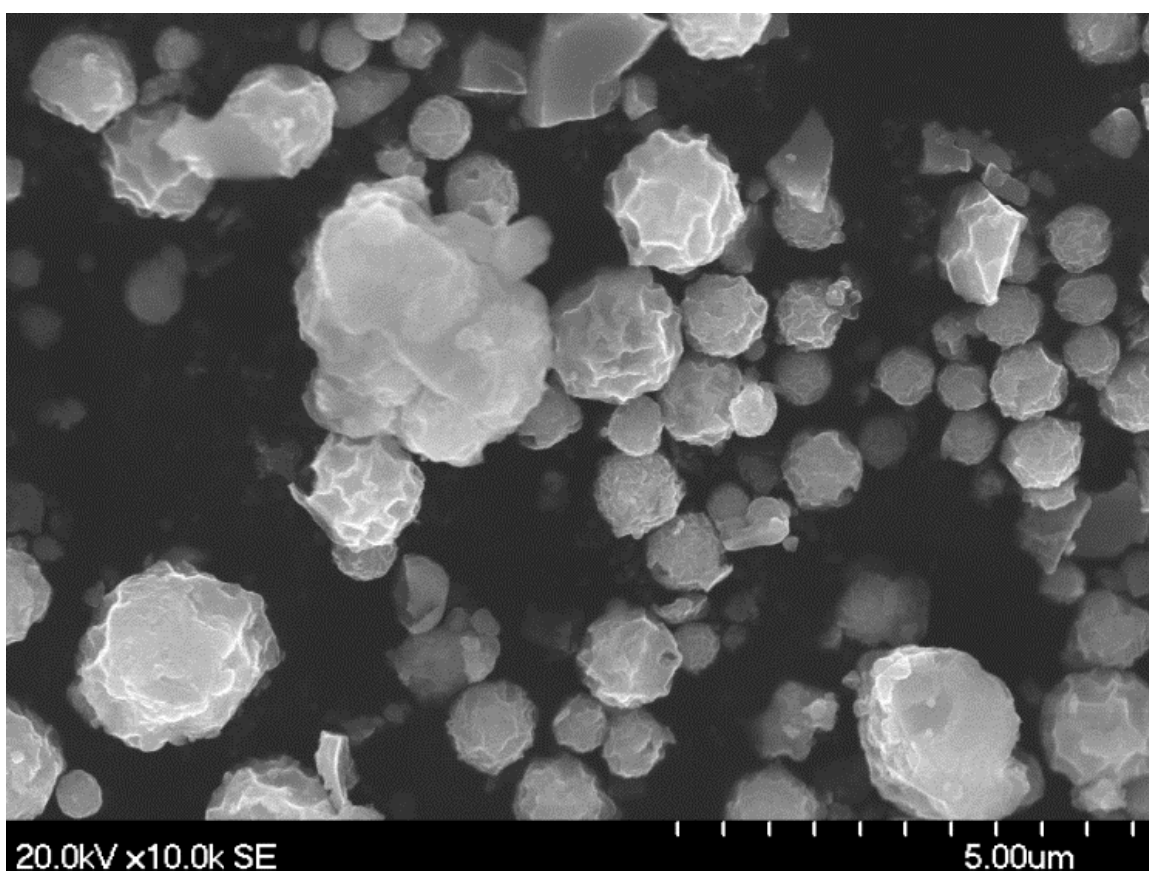


Figure 6. SEM image of as-prepared Pd<sub>2</sub>Zn.

Figure 7 shows the as-prepared material as seen in the SEM. This image shows irregular shaped particles ranging in size from approximately 0.5 μm to 2 μm. The irregular morphology is caused by the shrinking of the particles as the solvents evaporate

during drying in the furnace. As will be shown later, the particles seen in the SEM are composed of nano-scale crystallites.

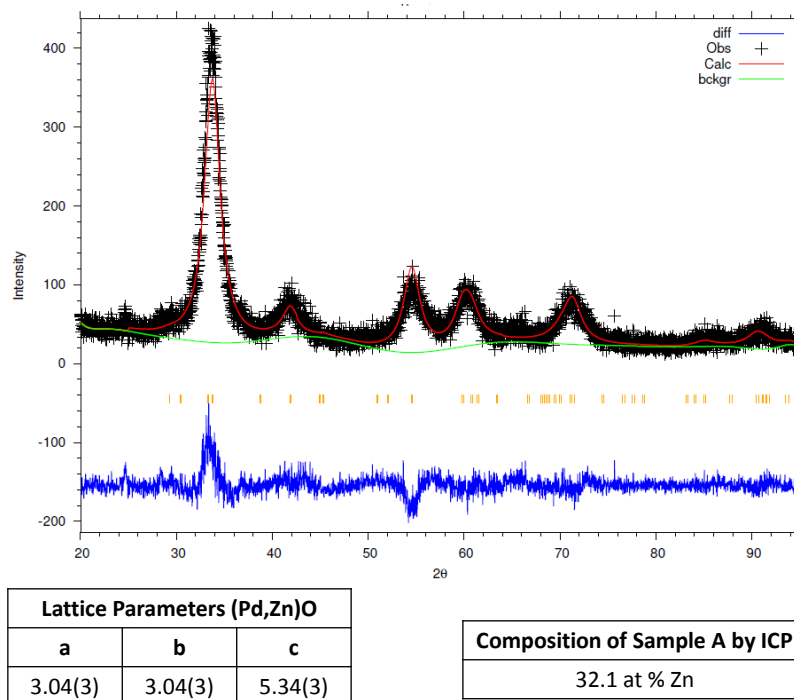


Figure 7. X-ray powder diffraction and Rietveld Refinement results for as-prepared Pd<sub>2</sub>Zn.

Figure 8 shows the XRD pattern of the as-prepared 2:1 oxide along with the Rietveld Refinement using the program GSAS. The tick marks below the pattern indicate the dominant PdO peaks as they appear from the ICSD recorded structure. The space group for this structure is P42/mmc, and the lattice parameters are  $a=3.03(1)$  Å and  $c=5.33(2)$  Å with a mean crystallite size of 4.5 nm. This powder contains both Pd and Zn as shown by EDS analysis, but we did not see any evidence of a separate ZnO phase. Therefore, we can conclude that the aerosol derived materials form a mixed oxide phase with Zn occupying Pd sites in the PdO lattice. Such a substitutional oxide is reasonable considering that the sizes of the Pd<sup>+2</sup> and Zn<sup>+2</sup> ions are similar in size.

Upon confirmation that a proper form of the starting material had been created, two aliquots of the sample were prepared for compositional analysis. The first was subjected to ICP analysis. The sample was dissolved in aqua regia. This analysis showed a composition of 32.1 atom% Zn for the as-prepared material of sample A. This is slightly low based on the initial solution, but it is within the composition range necessary for formation of the 2:1 phase.

The second aliquot was analyzed by thermogravimetric analysis. First, a small amount, on the order of 25 mg, was heated in air from room temperature to 1000°C. This was done as a means of confirming the composition of the sample given by ICP. Figure 9a shows two regions of mass loss as the sample was heated. The first mass loss around 200°C has been attributed to adsorbed water being removed from the sample. The high temperature mass loss at about 800°C is caused by the transformation of PdO into Pd.

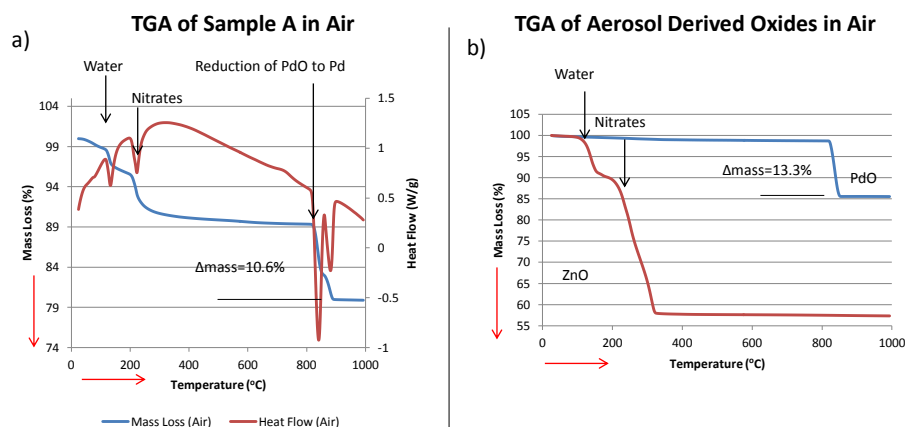


Figure 8. TGA analysis of sample A and reference PdO and ZnO in air.

TGA analysis of the reference PdO and ZnO are shown in Figure 9b. As the ZnO was heated, it shows the same low temperature mass loss at about 200°C, but no high temperature mass loss. As the PdO was heated, it showed no mass loss at 200°C, but a

significant mass loss above 800°C. This confirms that the mass loss at low temperatures can be attributed to the Zn portion of the sample. The stability of ZnO at high temperatures further indicates that the high temperature phase transformation of the Pd<sub>2</sub>Zn sample in air is solely attributed to the PdO portion of the sample. The second low temperature mass loss shown at approximately 200°C has been an unknown. ZnO is stable at these temperatures, so the hypothesis was that there were ligands left over from the precursor solutions, even though the furnace temperatures was believed to be high enough to decompose any nitrates during synthesis. In order to investigate this, an XRD pattern was gathered from the reference Zn oxide.

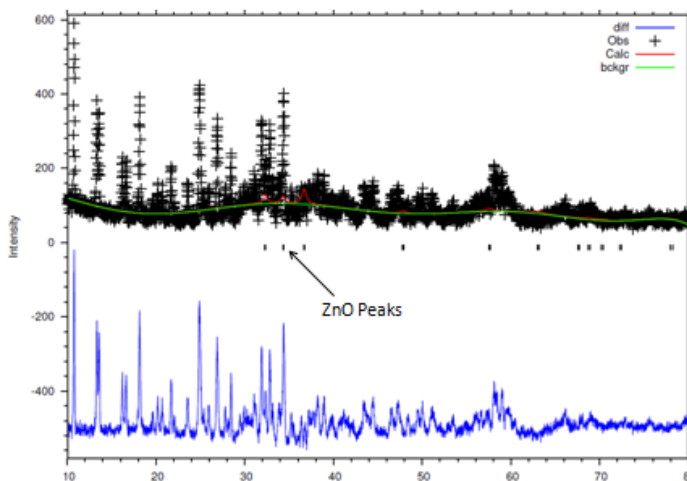


Figure 9. XRD of the reference Zn sample shows the absence of ZnO peaks indicating that the aerosol method actually produced Zn nitrate.

Figure 9 shows the XRD pattern of the reference Zn sample that was used for TGA analysis. The tick marks below the pattern indicate the angles at which ZnO peaks appear. The absence of these peaks in the pattern, and the abundance of peaks appearing at low angle indicate that the sample is composed of Zn nitrate as opposed to ZnO. The

presence of nitrates after synthesis indicates that the furnace temperature is not high enough to completely decompose ligands left by the precursors, or the residence time is not long enough. In either case, the results of the TGA studies conducted on this sample show that further treatment is needed after synthesis.

Another aliquot of this sample was treated in the TGA in  $H_2$ . This was done as a means of determining possible temperatures of phase transformation. In comparison with the TGA in air, the TGA in  $H_2$  shows a greater mass loss at low temperatures around  $200^\circ C$ . Although, this is in the same temperature at which we saw desorption of water and decomposition of nitrates from Zn, in  $H_2$  there is a far greater mass loss. We conclude is caused by PdO to Pd metal, which occurs at low temperatures in  $H_2$ . A second mass loss occurs about  $450^\circ C$ , indicating another phase transformation. In the data acquired at Brookhaven we saw that  $Pd_2Zn$  was formed at about  $450^\circ C$ , while PdZn formed at higher temperatures. Therefore, the subsequent experiments were performed at a temperature of  $450^\circ C$  and  $500^\circ C$ . Figure 10 shows the results of the TGA analysis in  $H_2$ . The reference samples in  $H_2$  show that both ZnO and PdO reduce at similar temperatures in this atmosphere, but unlike in air, Zn becomes volatile at high temperatures without the presence of Pd.

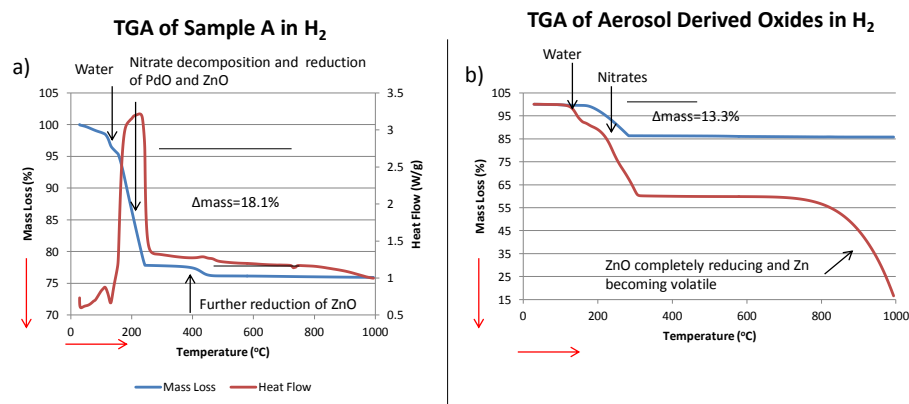


Figure 10. TGA analysis of Sample A and Reference PdO and ZnO in H<sub>2</sub>.

## 4.2 Sample Reduced in H<sub>2</sub> at 500°C

Figure 11 shows the x-ray diffraction pattern that from the sample treated at 500°C. Even though this sample was confirmed to be the proper stoichiometry to form the 2:1 phase, the product after heat treatment was not phase pure.

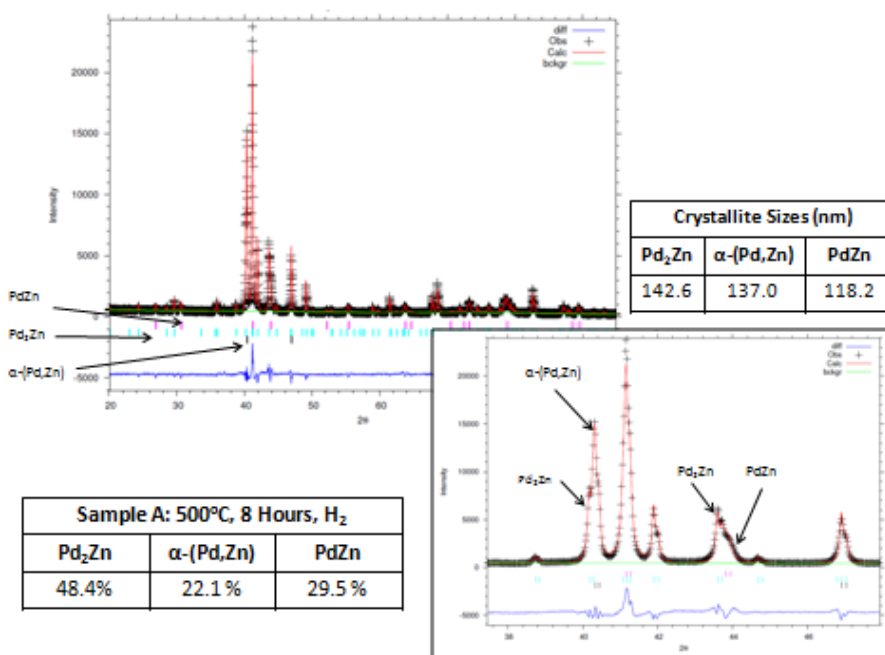


Figure 11. Figure 11. X-ray powder diffraction and Rietveld Refinement of sample A after eight hour reduction at 500°C in flowing H<sub>2</sub>.

Table 1. Structure and phase composition of sample A as determined by Rietveld Refinement.

Phase Information Sample A						
Pd <sub>2</sub> Zn		α-(Pd,Zn)		PdZn		
Weight Fraction						
48.4%		22.1 %		29.5 %		
33.3 at% Zn		10 at% Zn		50 at% Zn		
Composition by XRD				35.6at % Zn		
Lattice Parameters						
Orthorhombic		Cubic		Tetragonal		
<b>a</b>	5.338(9)	3.875(9)	2.924(5)			
<b>b</b>	4.154(7)	3.875(9)	2.924(5)			
<b>c</b>	7.752(3)	3.875(9)	3.32(3)			
Atomic Positions				Occupancies		Thermal Parameters
Site	x	y	z	Pd	Zn	
<b>Pd1</b>	0.039(5)	0.25	0.729(0)	1.0	0.0	0.0279
<b>Pd2</b>	0.1.70(5)	0.25	0.070(0)	1.0	0.0	0.0279
<b>Zn</b>	0.181(5)	0.25	0.404(7)	0	1.0	0.0279

Table 1 shows the structure and phase composition of Sample A after heat treatment.

Rietveld Analysis shows a phase composition of 48.4 at% Pd<sub>2</sub>Zn. XRD shows that there are three phases separate present in the sample, and the refinement gives relative amounts of each phase. This is consistent with previous work that shows the formation of PdZn at this temperature. Using the stoichiometry PdZn and Pd<sub>2</sub>Zn, and assuming a Zn contribution in the α-(Pd,Zn) phase an estimate of the composition can be made.

$$PdZn = 29.50g PdZn$$

$$Pd_2Zn = 48.42g Pd_2Zn$$

$$\alpha(Pd, Zn) = 22.08g \alpha(Pd, Zn)$$

$$29.50g PdZn \times \frac{1 mol PdZn}{171.8 g PdZn} \times \frac{1 mol Pd}{1 mol PdZn} = 0.1717 mol Pd; 0.1717 mol Zn$$

$$48.42g Pd_2Zn \times \frac{1 mol Pd_2Zn}{278.22 g Pd_2Zn} \times \frac{2 mol Pd}{1 mol Pd_2Zn} = 0.3481 mol Pd; 0.1740 mol Zn$$

$$22.08g \alpha(Pd, Zn) \times \frac{1 mol \alpha(Pd, Zn)}{(0.90(106.42) + 65.38)g \alpha(Pd, Zn)} \times \frac{0.90 mol Pd}{1 mol \alpha(Pd, Zn)}$$

$$= 0.1233 mol Pd; 0.0123 mol Zn$$

$$Total = 0.6431 mol Pd + 0.3358 mol Zn = 1.00 mol Total$$

$$atom\% Zn = \frac{0.3358 mol Zn}{1.00 mol Total} \times 100 = 33.6$$

The outcome of this calculation shows a composition of 33.6 at% Zn. Although, this is higher than expected, without knowing the exact composition of each phase present it is impossible to get an exact number. However, as an estimate this serves to indicate that the sample composition is reasonably close to the intended ratio.

Although, a mixed phase sample was not the desired outcome, Pd<sub>2</sub>Zn is present in a large enough phase fraction to isolate the structure. The only difficulty that had arisen from a non-phase pure sample was being able to refine the atomic occupancies. The occupancy parameter is refined through peak intensities, and some of the more intense  $\alpha$ -(Pd,Zn) and PdZn peaks overlap with Pd<sub>2</sub>Zn. In order to try and confirm the Rietveld structure a second sample was synthesized and reduced at a lower temperature.

### 4.3 Sample Reduced in H<sub>2</sub> at 450°C

Sample B was prepared using the same method and precursor solutions described above. After synthesis a portion of the sample was reduced at 450°C for four hours. Lowering the reduction temperature was done to inspect the behavior of the sample

closer to the 450°C mass loss shown in the TGA data. Treating the sample for a shorter reduction times was done in order to ensure that the sample was not forming, and then being destroyed as an effect of extended exposure to high temperatures. Figure 12 shows the pattern from this reduction. Visual inspection of the pattern shows both a presence of ZnO, and a dominance of  $\alpha$ -(Pd,Zn) in the sample. This indicates that a four hour reduction is insufficient to form the 2:1 phase.

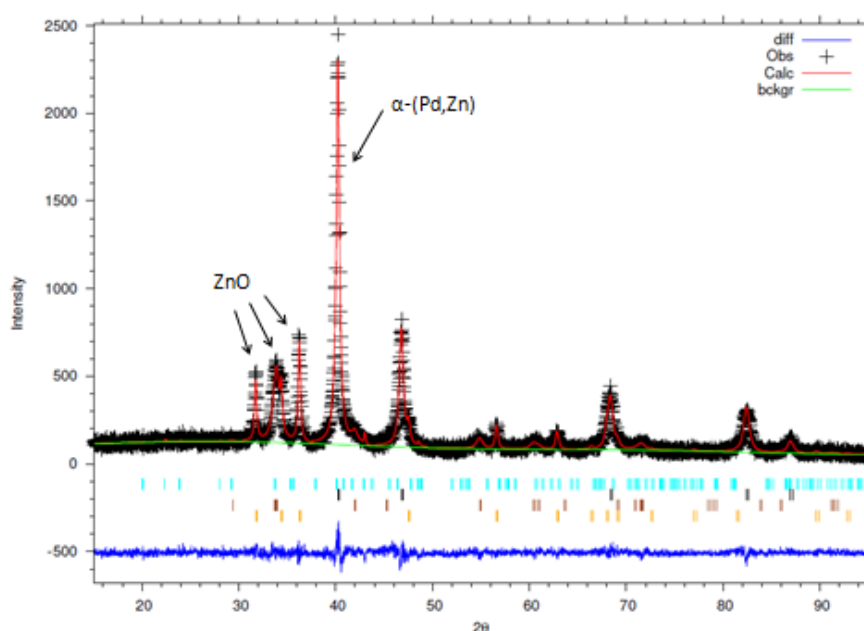


Figure 12. Sample B reduced for four hours at 450°C in flowing H<sub>2</sub>.

A second portion of the sample was reduced at 450°C for a full eight hours. Figure 13 is the diffraction pattern recorded from the eight hour reduction of sample B. The pattern shows noticeable differences in the peak intensities when compared to the 500°C reduction of sample A. The peaks of both  $\alpha$ -(Pd,Zn) and PdZn are much smaller, and the Pd<sub>2</sub>Zn peaks have increased in intensity. The XRD data from this sample was analyzed in the same manner as the pattern from Sample A.

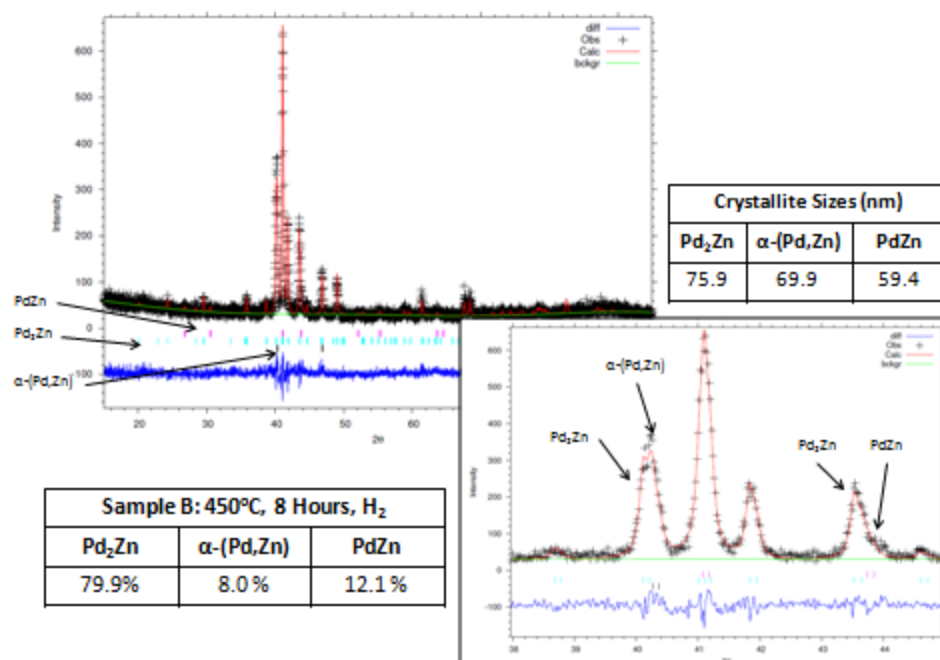


Figure 13. X-ray powder diffraction and Rietveld Refinement of sample B after reduction at 450C for eight hours in flowing H<sub>2</sub>.

Table 2. Structure and phase composition of Sample B as determined by Rietveld Refinement.

Phase Information of Sample B							
Pd <sub>2</sub> Zn		α-(Pd,Zn)		PdZn			
Weight Fraction							
79.9%		8.0%		12.1%			
33.3 at% Zn		10 at% Zn		50 at% Zn			
Composition by XRD				34.4 at% Zn			
Lattice Parameters							
	Orthorhombic	Cubic	Tetragonal				
a	5.338(9)	3.875(9)	2.924(5)				
b	4.154(7)	3.875(9)	2.924(5)				
c	7.752(3)	3.875(9)	3.32(3)				
Atomic Positions				Occupancies		Thermal Parameters	
Site	x	y	z	Pd	Zn		
Pd1	0.03(9)	0.25	0.72(6)	1.0	0.0		0.080
Pd2	0.16(8)	0.25	0.06(9)	1.0	0.0		0.080
Zn	0.18(2)	0.25	0.41(1)	0	1.0	0.080	

Table 2 shows the structure and phase compositions of this sample from Rietveld Refinement. The refinement confirms what the visual inspection of the peak intensities had indicated. The undesired phases have decreased in quantity, and the  $\text{Pd}_2\text{Zn}$  phase is present in a larger amount. This indicates that the temperature of formation for the 2:1 phase may be considerably lower than that of the 1:1, which is consistent with the synchrotron data that had originally prompted this study. Figure 14 illustrates the change in peak intensities between the refinements of reduced Sample A and reduced sample B.

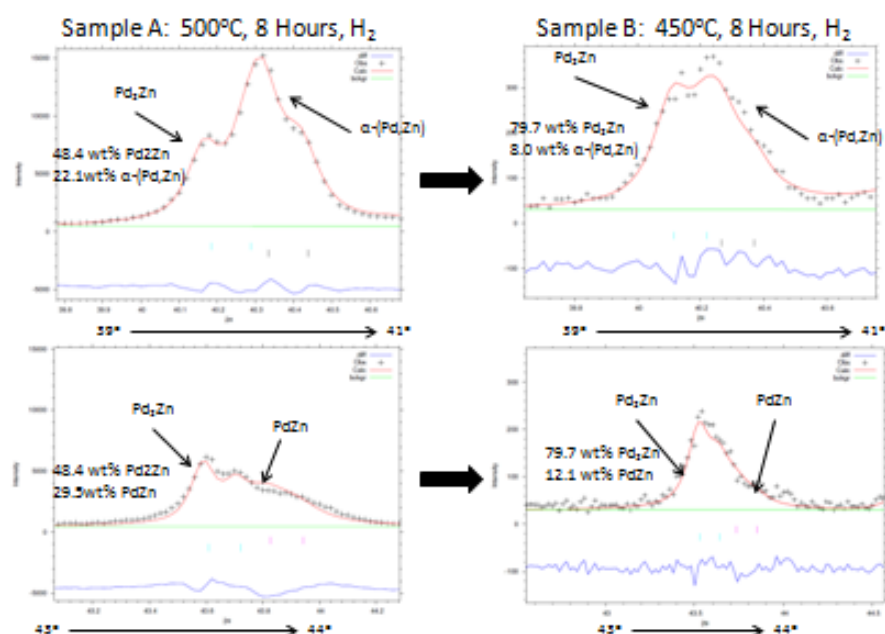


Figure 14. Comparison between the XRD patterns of sample A and sample B.

The compositional analysis of the oxide had proven that the precursor solutions had been mixed to the proper concentrations, so quantitative chemical analysis of sample B was started after heat treatment. In order to confirm that the composition of the reduced sample was consistent ratio with which the precursor solution was mixed electron microprobe analysis was conducted on the eight hour reduced sample. After reduction a portion of sample B was embedded, and cut on the ultramicrotome for TEM

analysis. The requirement of the sample that was embedded is minimal, so the remaining sample and epoxy stub were sealed in larger mold, and polished for microprobe analysis.

Figure 15 shows the outcome of this analysis.

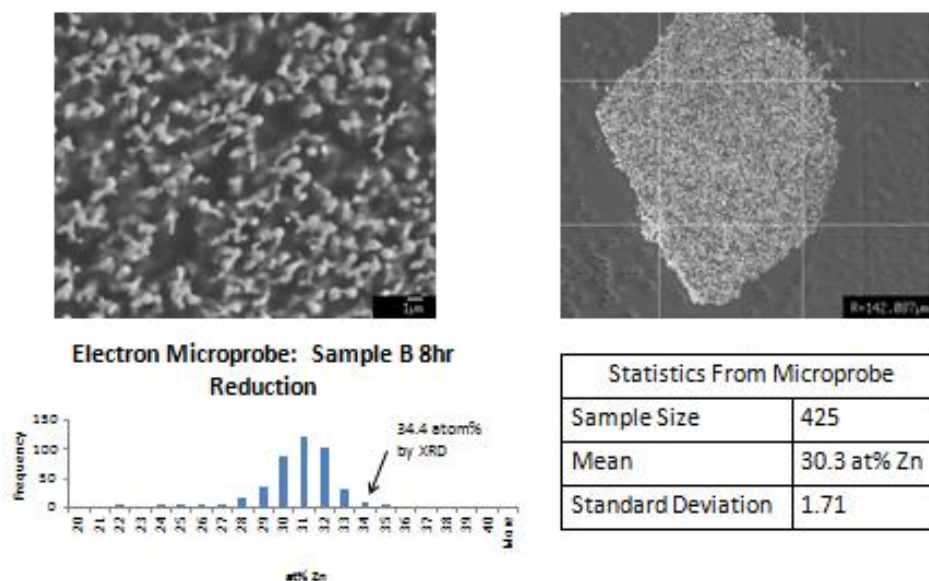


Figure 15. Electron microprobe analysis of Sample B after an eight hour reduction at 450C in flowing H<sub>2</sub>.

The microprobe analysis shows a composition of 30 at% Zn. Although, this is slightly lower than expected, it is in an acceptable range for forming the 2:1 phase. It should be noted, that Pd and Zn were the only elements used to calibrate the instrument. This may slightly affect the results as a 100% mass balance would not be able to be reached in areas that the beam hit that were not directly on a particle. However, the Pd and Zn ratios were most likely not affected by this, so the reports of the relative amounts of these two elements in the sample should be considered accurate.

As a final means of confirming the structure, the cross-sectioned samples were analyzed by the TEM. This is the novel characterization approach taken by this study.

Aerosol derived powders consistently present a problem when trying to analyze them using a TEM, it is difficult to obtain consistent electron diffraction data due to the diameter of the particles. The TEM requires that a sample be on the order of 20 nm thick to gather acceptable HRTEM images, and considerably thinner than that for lattice fringe analysis to be conducted. Lattice fringe studies of the 1:1 PdZn material have been performed, but these studies have always been limited to finding a thin region on the outer surface of a particle. Although, this can give an indication of the structure of a material at the surface, which is relevant for catalysts, it gives no insight into the sample's bulk structure.

Slicing the spherical particles into thin sections not only remedies the problem of particle thickness, but allows analysis of the particle's internal morphology. Although, the sectioned particles are still too thick for lattice fringe images to be taken, they are thin enough to gather selected area diffraction patterns. These patterns present a confirmation for the structure determined by XRD. Figure 16 shows a low magnification TEM image of the cross-sectioned sample.

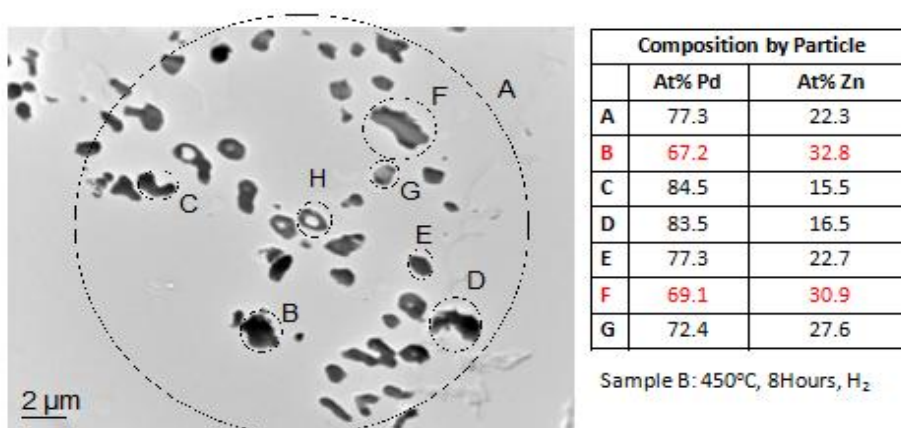


Figure 16. Low magnification TEM of sample B after being sectioned on an ultramicrotome.

The area in the large circle noted with the letter A shows the region that EDS was taken to determine an average composition of all of the particles in the image. This composition was determined to be 22.3 at% Zn, which is a lower Zn concentration shown by the previous analyses, but a sampling error had been noticed through the course of developing this technique. The cross-sectioning technique favored Pd heavy particles throughout the course of this study. The reason for this is unknown at this point, but future work to resolve this issue is planned.

Although, the EDS analysis was not useful in corroborating an average sample composition, it was useful in pinpointing particles of the 2:1 composition. The cross-sectioned images show particles of both the  $\text{Pd}_2\text{Zn}$  and  $\alpha\text{-(Pd,Zn)}$  compositions. Although, XRD had shown a presence of the 1:1 phase, particles of this composition were not evident in the cross-sectioned samples. Figure 17 shows the previous image with two particles, and their corresponding diffraction patterns.

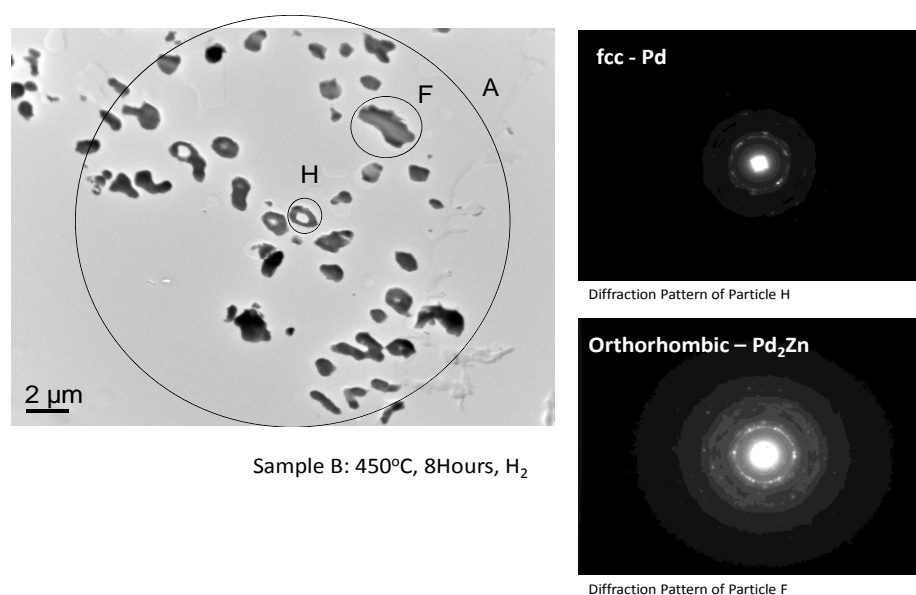


Figure 17. Comparison of the diffraction patterns of  $\alpha\text{-(Pd,Zn)}$  and  $\text{Pd}_2\text{Zn}$ .

The differences in structure and symmetry are readily apparent. The particles circled and marked with B and C were determined to have the  $\alpha$ -(Pd,Zn) and Pd<sub>2</sub>Zn compositions respectively. The figures below show the electron diffraction patterns of each of them.

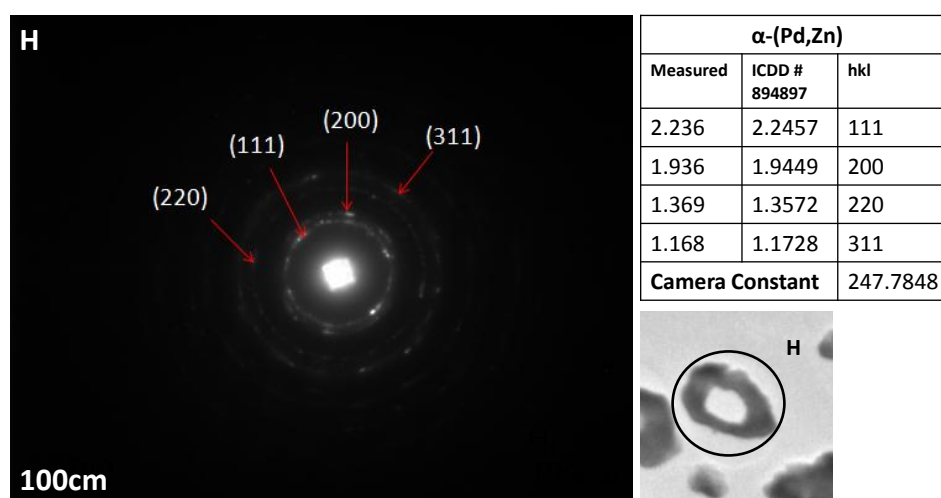


Figure 18. Indexing of the diffraction pattern of  $\alpha$ -(Pd,Zn)

Figure 18 shows the indexed diffraction pattern for the Pd rich particle denoted by B in the previous figure. The pattern was indexed using the standard ICDD structure for fcc Pd with the space group Fm-3m. The fact that the particles corresponding to this structure show an average Zn contribution of approximately 15 at%, but the structure indexes directly to Pd confirms that the material forms a solid solution of Pd and Zn in the fcc Pd structure at low Zn concentrations.

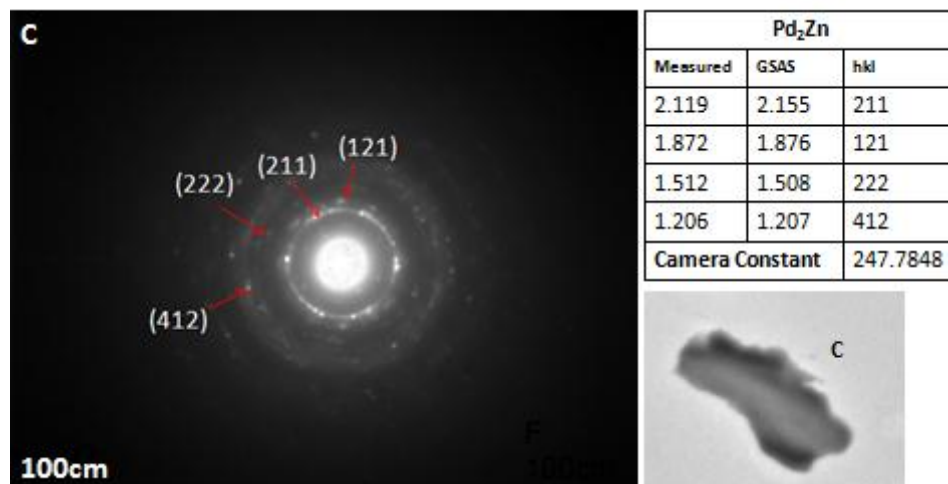


Figure 19. Indexing of the diffraction pattern cast by Pd<sub>2</sub>Zn.

The particle denoted as C in the TEM image was determined by EDS to have the 2:1 Pd<sub>2</sub>Zn composition. Figure 19 shows the pattern from this particle. The pattern was indexed to the Rietveld Refinement performed on the sample reduced for eight hours. The low symmetry structure of the Pd<sub>2</sub>Zn phase generates diffuse areas in the diffraction pattern that make indexing somewhat difficult. However, several planes that scatter more strongly than the rest can be seen in these regions of the pattern. These rings index to the structure determined by GSAS, corroborating the Pd<sub>2</sub>Zn structure.

## Conclusions

Although, a phase pure Pd<sub>2</sub>Zn sample has not been produced, the structure has been confirmed through XRD of two separate samples, and electron diffraction of the sample showing the highest phase purity. From a phase evolution stand point, it was determined that a multi-phase sample containing the Pd<sub>2</sub>Zn structure is formed after reduction in H<sub>2</sub> at 500°C for eight hours. However, the undesired phase contributions were very high at this reduction temperature. Furthermore, when the sample was reduced at 450°C, the presence of the 2:1 phase greatly increased. This implies that even though the stoichiometry was correct, a proper heat treatment is necessary to achieve the desired phase purity. At this point we do not know whether or not a phase pure sample can actually be produced.

TGA has shown that there is a phase transformation between 400°C and 450°C. This has been confirmed as a region of interest through the structural analyses performed on the samples in this study. As a higher phase fraction of the 2:1 structure was noticed after reduction at a lower temperature it stands to reason that there may be an exact time and temperature that will allow the Pd<sub>2</sub>Zn phase to form a phase pure material.

## Future Work

There is still work to be done to confirm if the Pd<sub>2</sub>Zn structure can be produced as a phase pure material using this method. The means of doing this should be to produce and characterize samples that have been heat treated at times and temperatures not discussed in this work. Ideally, this should be done at times between four and eight hours, and at temperatures in between 400°C and 450°C. Covering these times and temperatures should be sufficient to prove if the Pd<sub>2</sub>Zn phase is stable as a standalone structure.

The reasons for the sampling error noticed in the cross-sectioning method need to be identified. This method has proven very useful in analyzing the microstructure of large particles in the TEM. However, the material contained in the epoxy sections after processing is not compositionally representative of the entire sample. In the case of this study, the material that was viewed in the TEM was consistently Pd rich. In order to use this technique effectively for any phases that may be present, a means of preserving the presence of all sample phases after processing needs to be determined.

Finally, reactivity testing needs to be conducted on a sample containing a high concentration of Pd<sub>2</sub>Zn. It has been proven that out of the three phase regions that have been able to be produced by aerosol synthesis, that 1:1 PdZn is the only one to date that has been selective for MSR. As no one has conducted this testing on the 2:1 phase, it seems necessary to confirm its activity and selectivity.

## References

- Armbruster, M. (2010). Pd-Ga Intermetallic Compounds as Highly Selective Semi-Hydrogenation Catalysts. *Journal of American Chemical Society* , 14745-14747.
- Conant, T. (2008). Stability of bimetallic Pd-Zn catalysts for steam reforming of methanol. *Journal of Catalysis* , 64-70.
- Dyer, C. (2004). Fuel cells and portable electronics. *Symposium on VLSI Circuits Digest of Technical Papers*, (pp. 124-127).
- Dyer, C. (2002). Fuel cells for portable applications. *Journal of Power Sources* , 31-34.
- Farrauto, R. J. (2011). A PdZn catalyst supported on stabilized ceria for stoichiometric methanol steam reforming and hydrogen production. *Applied Catalysis A: General* , 64-70.
- Halevi, B. (2010). Aerosol Derived Bimetallic Alloy Powders: Bridging the Gap. *Journal of Physical Chemistry C* , 17181-17190.
- Halevi, B. (2012). Catalytic reactivity of face centered cubic PdZn for the steam reforming of methanol. *Journal of Catalysis* , 44-54.
- Iwasa, N. (2003). Effect of Zn addition to supported Pd catalysts in the steam reforming of methanol. *Applied Catalysis A* , 153-160.
- Kawamura, Y. (2006). A miniaturized methanol reformer with Si-based microreactor for a small PEMFC. *Chemical Engineering Science* , 1092-1101.
- Peterson, E. J. (2010). Aerosol Synthesis and Rietveld Refinement of tetragonal (B1) PdZn. *Journal of Alloys and Compounds* .
- Stadelmaier, H. H. (1963). Tenare Kohlenstofflegierungen von Palladium and Platin mit Magnesium, Aluminum, Zink, Gallium, Germanium, Kadmium, Indium, Zinn, Quecksilber, Thallium, and Blei. *Acta Metalurgica* , 415-419.